Spatio-temporal organization of cell assemblies in Nucleus Reuniens during slow oscillations.

David Angulo-Garcia[1,*] , Maëva Ferraris[2,*], Antoine Ghestem[2], Christophe Bernard[2], Pascale P Quilichini[2]

[1] Grupo de Modelado Computacional. Instituto de Matematicas Aplicadas, Universidad de Cartagena, Cartagena, Colombia

[2] Aix Marseille Univ, INSERM, INS, Inst Neurosci Syst, Marseille, France

[*] *These authors contributed equally*

Abbreviated Title: Sequences in Nucleus Reuniens

Corresponding Author:

Pascale P Quilichini

Institut de Neurosciences des Systèmes - INSERM U1106- Aix-Marseille Université

Faculté de Médecine - Campus Santé Timone

27 bd Jean Moulin - 13005 Marseille - France

Tél : +33 (0)4 91 32 42 31 - Fax : +33 (0)4 91 78 99 14

Email: pascale.quilichini@univ-amu.fr

Keywords:

Cell assemblies; Hippocampus; Prefrontal cortex; Nucleus reuniens; Slow oscillations; Sequences.

Acknowledgments:

This work was supported by grants from the FRM (Fondation Recherche Médicale FDT201805005246 to M. F.). D.A-G was received support by the A*MIDEX grant (No. ANR-11-IDEX-0001-02). We thank Wesley Clawson for proofreading this manuscript.

Author Contributions:

M.F. and P.P.Q. designed the experiments. M.F. and P.P.Q. performed the experiments. A.G. assisted in performing experiments. D.A.G., M.F. and P.P.Q. interpreted the results and performed the analysis. All the authors reviewed and edited the manuscript.

Declaration of Interests:

The authors declare no competing interests.

Abstract The nucleus reuniens (NR) is an important anatomical and functional relay between the medial prefrontal cortex (mPFC) and the hippocampus (HPC). Whether the NR controls neuronal assemblies - a hallmark of information exchange between the HPC and mPFC for memory transfer/consolidation - is not known. Using simultaneous LFP and unit recordings in NR, HPC and mPFC in rats during slow oscillations under anesthesia, we identified a reliable sequential activation of NR neurons at the beginning of UP states, which preceded mPFC ones. NR sequences were spatially organized, from dorsal to ventral NR. Chemical inactivation of the NR disrupted mPFC sequences at the onset of UP states as well as HPC sequences present during sharp-wave ripples. We conclude that the NR contributes to the coordination and stabilization of mPFC and HPC neuronal sequences during slow oscillations, possibly via the early activation of its own sequences.

Introduction

Information exchange between the hippocampus (HPC) the medial prefrontal cortex (mPFC) is essential for different memory processes, including consolidation **(Siapas and Wilson, 1998, Frankland and Bontempi, 2005, Maingret et al., 2016, Eichenbaum, 2017, Kitamura et al., 2017, Latchoumane et al., 2017, Preston and Eichenbaum, 2013)**. In both regions, the representation of information is supported by the recruitment of cell assemblies of neurons which fire in a fine time-resolved manner **(Lee and Wilson, 2002, Euston et al., 2007, Luczak et al., 2007, Pastalkova et al., 2008, Luczak et al., 2015, Peyrache et al., 2009, Battaglia et al., 2011, Skaggs and McNaughton, 1996, Nadasdy et al., 1999)**. These neuronal assemblies display a precise temporal sequential activation, which reflects the encoded information **(Pfeiffer, 2017, Marre et al., 2009, Davidson et al., 2009, Foster and Wilson, 2006, Ji and Wilson, 2007, Nádasdy, 2000)**. Such activity occurs mainly during sleep, particularly during non-REM sleep, and is organized in space and time by a set of oscillations, such as hippocampal sharp-wave ripples, cortical slow oscillations and spindles **(Sirota et al., 2003, Sirota and Buzsáki, 2005, Maingret et al., 2016, Staresina et al., 2015)**. Yet, how these cells assemblies are finely coordinated between HPC and mPFC to support memory consolidation is not well understood. The thalamic nucleus reuniens (NR), which bi-directionally connects the HPC and mPFC **(Herkenham, 1978, Van der Werf et al., 2002, Vertes, 2006, Varela et al., 2014)**, plays a key role in memory consolidation **(Loureiro et al., 2012, Cassel et al., 2013, Pereira de Vasconcelos and Cassel, 2015)**, and synchronizes gamma bursts between HPC and mPFC during non-REM sleep **(Ferraris et al., 2018)**. The NR is therefore ideally posed to orchestrate the dynamics of cell assemblies in both regions.

Results

Cell assemblies are recruited in NR at UP state onset

We first assessed the behavior of NR (n=166 cells, n=5 rats), mPFC (n=496, n=7) and HPC (n=163, n=4) neurons during slow oscillations (SO) in anesthetized rats. Slow oscillations during anesthesia share similar features as non-REM sleep **(Ferraris et al., 2018)** and offer the advantages of long duration stable recordings necessary to identify statistically significant sequences. Neighboring thalamic neurons (antero-median and ventro-median nuclei) were also recorded as a control group ("TH", 89 neurons, n=4).

During SO, most of the neurons fired at the onset of the UP states, mainly in mPFC and NR (Figure 1A) **(Ferraris et al., 2018)**. To identify any ordering in this firing activity, we ranked each neuron according to its mean preferred SO phase (Figure 1Ba). Neurons were organized in increasing order of average preferred phase, defining a *template order* (Figure 1Bb). With this ordering, we found a robust recruitment of neuronal sequences at the UP state onset in NR (median percentage of recruited neurons per UP state 70.35 %, min/max: 61.13 / 85.85 %), and mPFC (median: 62.9 %, min/max: 42.06 / 70.02 %). In comparison, HPC neurons showed less sequential activation (median: 33.82 %, min/max: 29.26 / 46.42 %, Figure 1B). However, HPC neurons displayed better sequential activation during sharp wave ripples (SPW-Rs), which tend to occur at the end of the SO cycle **(Sirota et al., 2003, Isomura et al., 2006, Buzsáki, 2015, Khodagholy et al., 2017, Battaglia et al., 2004, Maingret et al., 2016)** (median: 45 %, min/max: 35 / 64 %)**.** Sequences in NR always preceded mPFC ones (Figure 1B). As a negative control, we analyzed the activity of neighboring thalamic nuclei (TH) neurons. Although TH neurons displayed a strong entrainment by SO **(Ferraris et al., 2018)**, there was poor sequential activity (Figure 1B). The sequential activity at UP state onset therefore appears to be specific of NR and mPFC neurons in the areas investigated here. As a further control, we analyzed the

activity of NR neurons during epochs dominated by theta (4-6 Hz) oscillations. We did not find stable sequential neuronal assemblies during theta (data not shown). Together, these results show that, at the beginning of UP states, cell assembly formation occurs first in NR, then in mPFC and marginally in the HPC and neighboring thalamic nuclei.

We then quantified the reliability of these sequences. To do so, we computed at each UP state the activation latency of each neuron relative to the population peak activity (**see Methods**). The local activation order of the cell assembly was determined from the ascending sorting of the activation latencies. We then measured the Spearman rank correlation between the local activation order and the template order. A rank correlation r = 1 indicates that the sequential activation follows exactly the template order determined previously by the average phase preferences. For NR neurons, the template order was significantly expressed in 32% of the total number of UP states (min = 15%, max = 37 %, Spearman test, $p < 0.01$), while mPFC reliable sequences were found in only 25 % of the UP states (min/max = 5 / 31 %, **Figure 1C**). In contrast, reliable HPC sequences were only detected in 2 % of UP states (min/max = 1 / 6 %) and in 2 % for sequences in TH neurons (min/max = 1 / 14 %). Although the proportion of reliable sequences in NR and mPFC were not significantly different (KS-test, $p = 0.15$), the average Spearman correlation values of the reliable sequences were significantly larger in NR than in mPFC (KS-test, $p < 0.01$, **Figure 1D**), indicating that the NR cell assembly sequential organization is the most consistent. To estimate the participation of neurons in sequence generation, we calculated a participation index, defined as the probability for a given neuron to be involved in a given sequence (see Methods). The participation index was consistently larger across experiments in NR (median: 0.63, min/max: 0.55 / 0.81) than in mPFC (median: 0.52, min/max: 0.36 / 0.60; KS-test, $p < 0.05$). Thus, mPFC and NR are characterized by highly stable

patterns of sequential neuronal activations at the onset of the UP state, with NR sequences being more reproducible.

NR cell assemblies are spatially distributed

We also investigated the spatial distribution of the NR and mPFC cells assemblies. For each UP state, we correlated the local activation order of each neuron to their anatomical dorso-ventral localization (**Figure 2A**). The slope of a linear fit of such correlation provides the information on whether the activity is propagating in a given direction **(Luczak et al., 2007)** (see Methods, **Figure 2B**). Even though both NR and mPFC can show some degree of propagation in a preferential direction, NR average slopes were consistently larger than mPFC ones (KS-test, $p < 0.05$, **Figure 2C**), reflecting a dorsal-to-ventral direction of propagation of the neuronal activations. To assess the consistency of the preferential direction of propagation, we calculated the Spearman rank correlation between the rank of the template order and the anatomical location of the corresponding recording site. We found a highly significant correlation in NR recordings in most cases ($n = 4$ out of 5, median $|r|$ value across all n: 0.65, $p < 0.001$), whereas it was virtually absent in mPFC ($n = 1$ out of 7, $|r| = 0.35$, $p < 0.01$) (**Figure 2D**). There are thus more spatially organized sequences in NR as compared to mPFC (z-test, $p < 0.05$, **Figure 2E**).

Altogether, these results demonstrate that NR displays at the UP state onset robust sequential activations which are spatially organized in a dorso-ventral stream. This is particularly surprising as it suggests a topical spatial organization of the neuronal output in the NR.

NR activity is necessary to the mPFC and HPC sequences stability

The fact that NR cell assemblies are generated before mPFC and HPC ones raises the possibility that NR neurons may control mPFC and HPC sequences. To test this hypothesis, we

134 performed chemical inactivation of NR using Muscimol (see Methods) and recorded the activity
135 of mPFC neurons (n=140, n=3) and HPC (n=71, n=3) neurons. Following NR inactivation, mPFC
136 neurons showed a less rich activity during the UP state as compared to non-inactivation, control
137 recordings (Figure 3A) **(Ferraris et al., 2018)**. A hallmark of highly active, long-lasting firing of
138 cells in control conditions is the broad distribution of inter-spike intervals (ISI) smaller than 0.5 s.
139 The distribution was much narrower in inactivation conditions (Figure 3B). We then calculated
140 the distribution of the pooled variability of the activity peak triggered histogram (APTH, see
141 methods and Figure 3C insert) in control and NR inactivation conditions. The median APTH
142 variability across experiments was consistently lower when NR is inactivated (control median:
143 9.62, min/max: 8.98 / 10.60, NR inactivation median: 8.92, min/max: 8.67 / 9.02, KS-test, $p<0.05$),
144 as shown in Figure 3C. Moreover, the UP state duration was slightly shorter (control: 0.55 s, NR
145 inactivation: 0.48 s, Mann-Whitney test, $p < 0.001$), as revealed by the extra peak in UP state
146 duration distribution around 0.25 s, which did not exist in control data (Figure 3D). We then
147 evaluated the outcome of the mPFC sequences in such conditions. First, NR activity suppression
148 resulted in a reduced capacity of mPFC to generate reliable sequences as compared to control
149 condition since only 6.5% of them (min = 4.0% max =8.4%) were reliable (as compared to
150 control median: 25%, min/max: 5 / 30 %, KS-test, $p<0.05$ Figure 3E). Moreover, the fraction of
151 participating neurons in reliable sequences decreased in such condition (control: 53%;
152 inactivation: 38%; KS-test, $p < 1e-5$; Figure 3F). These results support the proposal that NR
153 controls the stability and reliability of mPFC sequences.

154 The UP state of the SO poorly modulates the activity of HPC neurons and the formation of timely
155 organized cell assemblies, however, SPW-Rs are more likely to trigger a sequential activation of
156 HPC firing **(Buzsáki, 2015)**. We therefore investigated the consequences of NR inactivation on
157 HPC sequences during SPW-Rs. NR inactivation did not affect HPC neurons firing rate (control

158 median: 70 Hz, min/max: 41 / 85 Hz, NR inactivation median: 52.59 Hz, min/max: 33 / 71 Hz,
159 KS-test, p=0.97, **Figure 4A**). In addition, NR inactivation did not alter the frequency of SPW-Rs
160 occurrence (median control: 0.087 Hz, min/max: 0.043 / 0.11 Hz, NR inactivation: 0.029 Hz,
161 min/max: 0.022 / 0.049 Hz, KS-test, p=0.32, **Figure 4B**). Similarly, neither their power (mean
162 normalized power control: 157 ± 2, NR inactivation: 144 ± 5, T-test, p=0.295; Figure 4C bottom
163 panel) nor their inner frequency (mean frequency control: 193 ± 1 Hz, NR inactivation: 213 ± 3
164 Hz, T-test, p=0.084, **Figure 4C** top panel) were modified. In contrast, the number of reliable
165 sequences found within SWP-Rs was drastically reduced (control median: 20%, NR inactivation
166 median: 2%, z-test, p<0.001; **Figure 4D**). Besides, the remaining cell assemblies recruited a
167 significantly lower number of neurons (control median: 37.5 %, min/max: 12.5% / 80%, NR
168 inactivation median: 8.3 %, min/max: 0% / 66.7%, KS-test, p<0.001, **Figure 4E**). These findings
169 support the proposal that NR also controls the sequential organization of neuronal firing in HPC
170 during SWP-Rs.

171 Discussion

172 In this study, we showed that ⅔ of NR neurons fire within robustly spatially and temporally
173 organized cell assemblies at UP state onset; and that NR activity controls cell assemblies'
174 stability in mPFC at UP state onset and in HPC during SPW-Rs. These results further support the
175 concept that the NR is a key functional hub in memory networks involving the medial prefrontal
176 cortex and hippocampus.

177 The sequential activation of neuronal assemblies constitutes a core feature of information
178 processing in the brain **(Tonegawa et al., 2018)**. Cell assemblies are found in archicortical **(Lee**
179 **and Wilson, 2002, Pastalkova et al., 2008, Villette et al., 2015, Malvache et al., 2016, Harris**
180 **et al., 2003, Dragoi and Buzsáki, 2006)** and cortical areas **(Euston et al., 2007, Luczak and**

Maclean, 2012, Luczak et al., 2007, Kenet et al., 2003, MacLean et al., 2005, Ferezou et al., 2006) (as well as in striatum **(Lansink et al., 2009)**). They constitute a way to code/encode/store information **(Maass, 2016, Kitamura et al., 2017)**. During non-REM sleep, cortical activity is dominated by the sequential activation of cortical neurons at the onset of the UP state, while, in the hippocampus, the sequential activation mostly occurs during SPW-Rs at the end on the slow oscillation cycle **(Sirota et al., 2003, Battaglia et al., 2004, Maingret et al., 2016, Khodagholy et al., 2017, Peyrache et al., 2009)**. Similar sequential firing occurs during the slow oscillations measured during anesthesia **(Luczak et al., 2007)**, supporting the view that such brain state shares many features with non-REM sleep **(Tung and Mendelson, 2004, Clement et al., 2008, Isomura et al., 2006, Quilichini et al., 2010, Hutt, 2011, Ferraris et al., 2018)**. Whether sequences represent internally generated representations or preconfigured cell assemblies **(Pastalkova et al., 2008, Dragoi and Tonegawa, 2012, Liu et al., 2018)** or a functional template of offline replay in the framework of memory consolidation **(Buzsáki, 2015, Lee and Wilson, 2002, Pfeiffer, 2017)** still remains to be elucidated, yet this work shows that they can also be recorded during anesthesia in this thalamic nucleus **(Bermudez Contreras et al., 2013)**. The way mPFC and HPC sequences are generated remains poorly understood. Our results demonstrate that NR activity is a key regulator of mPFC and HPC sequence stability. Although the basic dynamical properties of UP states and SPW-Rs were mostly not affected by NR activation, mPFC and HPC sequences were considerably disrupted. The NR is ideally located for this, as it is bi-directionally connected to the mPFC and HPC **(Vertes, 2006, Cassel et al., 2013, Varela et al., 2014)**. The fact that NR sequences always precede mPFC ones at UP state onset suggests that NR cells may directly drive mPFC cells. In keeping with this proposal, NR neurons have an excitatory action on HPC and mPFC **(Dolleman-Van der Weel et al., 1997, Dolleman-Van der Weel and Witter, 2000, Di Prisco and Vertes, 2006)** by

205 modulating/activating both interneurons and principal cells. However, the control of sequences
206 during hippocampal SPW-Rs is more difficult to explain as SPW-Rs occur at variable times after
207 UP state onset **(Sirota et al., 2003, Battaglia et al., 2004)**.
208 The presence of sequences specifically in the NR is quite remarkable (sequences were not
209 found in neighboring thalamic nuclei). Since NR neurons are involved in reference memory
210 consolidation **(Loureiro et al., 2012)** and in spatial memory **(Jankowski et al., 2014, Ito et al.,**
211 **2015, Jankowski et al., 2015, Ali et al., 2017, Cholvin et al., 2018)**, NR sequences may
212 constitute an activity template used to organize information at the beginning of the UP state (i.e.
213 a default activity in a default mode **(Sanchez-Vives and Mattia, 2014)**), in order to transmit it to
214 the target areas in a packet-based manner **(Luczak et al., 2015)**.
215 Another remarkable feature of NR sequences is that their dorso-ventral organization, suggesting
216 a precise topological organization in terms of afferences and efferences, despite the fact that NR
217 does not have a layered organization **(Jones, 1985, Bokor et al., 2002, Van der Werf et al.,**
218 **2002)**. Studies report topographically (dorso-ventral) organized inputs to NR (from subiculum
219 **(Van der Werf et al., 2002, McKenna and Vertes, 2004)**, but most of the differences involve
220 the rostro-caudal axis **(Cassel et al., 2013)**. However, a fuzzy dorso-ventral gradient has been
221 reported on the NR output to the temporal lobe **(Dolleman-Van Der Weel and Witter, 1996,**
222 **Vertes et al., 2006)**. There is also no available information on the local connectivity among NR
223 neurons, except a caudal to rostral pathway **(Dolleman-Van der Weel et al., 1997)**. The NR
224 includes difference cell types, but the lack of specific molecular markers prevents, so far, a
225 proper optogenetic investigation **(Bokor et al., 2002, Walsh et al., 2017)**.

226 In conclusion, our results further support the concept that the NR plays a key role as an
227 anatomical and functional hub between the mPFC and HPC. The control it exerts on mPFC and
228 HPC information packets suggests that it strongly participates in the organization of information

in both regions but also in the transfer of information from the HPC to mPFC. Its internal organization allows the genesis of information packet sequences, which may represent similar features as those coded in the mPFC and HPC.

Materials and Methods

Contact for Reagent and Resource Sharing

Further information and requests for resources may be directed to and will be fulfilled by the Lead Contact, Dr. Pascale P. Quilichini (pascale.quilichini@univ-amu.fr).

Key Resources Table

Reagent type (species) or resource	Source	Identifier
Animals		
Wistar Han IGS rats	Charles River	RRID:RGD_2308816
Chemicals		
Urethane	Sigma-Aldrich	Cat#U2500; CAS: 51-79-6
Isoflurane	Baxter	CAS: 26675-46-7
Ketamine	Renaudin	Cip: 3400957854195
Xylazine	CENTRAVET	Cat#ROM001 CAS: 7361-61-7
Sodium pentobarbital	CEVA	CAS: 76-74-4
Paraformaldehyde	Carlo Erba	Cat#387507 CAS: 30525-89-4
NeuroTrace 500/5225 Green Fluorescent Nissl Stain	Invitrogen	Cat#N21480
Muscimol BODIPY TMR-X Conjugate	Invitrogen	Cat#M23400
DiIC18(3)	Interchim	Cat#46804A CAS: 41085-99-8
Software and Algorithms		
MATLAB v2013b	MathWorks	RRID:SCR_001622
MATLAB v2015b	MathWorks	RRID:SCR_001622

Circular Statistics Toolbox	https://philippberens.wordpress.com/code/circstats/	Berens, P. (2009).
KlustaKwik	http://klustakwik.sourceforge.net Harris et al., 2000	RRID:SCR_008020 RRID:SCR_014480
Klusters	http://neurosuite.sourceforge.net Hazan et al., 2006	RRID:SCR_008020
NeuroScope	http://neurosuite.sourceforge.net Hazan et al., 2006	RRID:SCR_008020
NDManager	http://neurosuite.sourceforge.net Hazan et al., 2006	RRID:SCR_008020
Other		
Digital Neuralynx recording system (32 kHz sampling)	Neuralynx	Model: 64-channel Digital Lynx
Pulse oximeter	Starr life sciences	MouseOx
Motorized manipulator	Scientifica	Scientifica IVM single
Silicon probe 32 aligned sites (177µm2), 20µm spacing, 50µm thick,10mm long	NeuroNexus	A1x32-Edge-10mm-20-177-H32-50
Silicon probe 32 aligned sites (177µm2), 20µm spacing, 15µm thick, 5mm long	NeuroNexus	A1x32-Edge-5mm-20-177-H32-15
Silicon probe 32 aligned sites (177µm2), 50µm spacing, 15µm thick, 6mm long	NeuroNexus	A1x32-6mm-50-177-H32-15
Vibratome	Leica	VT1000S
Stereotaxic frame	Kopf	#962
Syringe 75RN 5µl	Hamilton	Cat#87930
Needle 33 gauge	Hamilton	Cat#7803-05
UltraMicroPump	World precision instrument	UMP3-1

Experimental Model and Subject Details

All experiments were performed in accordance with experimental guidelines approved by Aix-Marseille University Animal Care and Use Committee. A total of 16 rats were used in this study. Part of these data (14 Wistar Han rat data) were used in a previously published study **(Ferraris et al., 2018)**, and 2 Wistar Han rats are original data. They include local field potentials (LFPs) and single-unit recordings made in the mPFC, HPC and NR of anesthetized rats.

Animal surgery

Wistar Han IGS male rats (250-400g; Charles River) were anesthetized with urethane (1.5 g/kg, i.p.) and ketamine/xylazine (20 and 2 mg/kg, i.m.), additional doses of ketamine/xylazine (2 and 0.2 mg/kg) being supplemented during the electrophysiological recordings. The heart rate, breathing rate, pulse distension and the arterial oxygen saturation were also monitored with an oximeter (MouseOx, Starr Life Science) during the entire duration of the experiment to ensure the stability of the anesthesia and monitor the vital constants. The head was secured in a stereotaxic frame (Kopf, Phymep) and the skull was exposed and cleaned. Two miniature stainless-steel screws, driven into the skull, served as ground and reference electrodes. Up to three craniotomies were performed to target, from bregma: the pre-limbic area of the medial prefrontal cortex (mPFC) at +3 mm AP and +0.8 mm ML; the CA1 field of the intermediate hippocampus (HPC) at -5.6 mm AP and +4.3 mm ML; and the nucleus reuniens (NR) at -1.8 mm AP and -2 mm ML. Silicon probes (NeuroNexus) were used to record from these structures: a A1x32-Edge-5mm-20-177-H32-15 probe placed at [-2.5 -3.1] mm from brain surface to reach mPFC layer 5; a A1x32-Edge-10mm-20-177-H32-50 32-site probes placed at -7.2 mm from brain surface to reach the NR; a HPC A1x32-6mm-50-177-H32-15 probe placed at [-2.8 -3.0] mm perpendicularly to the CA1 field from stratum oriens to stratum lacunosum moleculare in the HPC. All the probes were lowered inside the brain with a motorized manipulator (Scientifica). For the NR inactivation experiments (n = 3 rats), a local injection of a fluorophore-conjugated muscimol (BODIPY-MSCI TMR-X Conjugate, Invitrogen) was performed in the NR and data from the mPFC and the HPC (CA1) were simultaneously acquired. The injection needle (33 gauge, Hamilton) was inserted in the NR (using the same depth coordinates as the probes and mounted on the same micromanipulator) and 0.70 nmol of muscimol in 0.3 µl of PBS **(Ferraris et al., 2018)** was delivered over 60s through a micropump (UltraMicroPump, WPI). The needle was left

in place for 3 additional minutes to allow for adequate diffusion of the drug, then carefully removed.

At the end of the recording, the animals were injected with a lethal dose of Pentobarbital Na (150mk/kg, i.p.) and perfused intracardially with 4% paraformaldehyde solution in phosphate buffer (0.12M). The position of the electrodes (DiIC18(3), InterChim) was applied on the back of the probe before insertion) was confirmed histologically on Nissl-stained 60 µm sections (NeuroTrace 500/5225 Green Fluorescent Nissl Stain, Invitrogen). Only experiments with appropriate position of the probe were used for analysis (Figure 2A).

Data collection and initial analysis

Extracellular signal recorded from the silicon probes was amplified (1000x), bandpass filtered (1 Hz to 5 kHz) and acquired continuously at 32 kHz (64-channel DigitalLynx; NeuraLynx) at 16-bit resolution. Raw data were preprocessed using a custom-developed suite of programs **(Csicsvari et al., 1999)**. After recording, the signals were downsampled to 1250 Hz for the local field potential (LFP). Spike sorting was performed automatically, using KLUSTAKWIK (Harris et al., 2002), followed by manual adjustment of the clusters, with the help of autocorrelogram, cross-correlogram and spike waveform similarity matrix (KLUSTERS software, **(Hazan et al., 2006)**. After spike sorting, the spike features of units were plotted as a function of time, and the units with signs of significant drift over the period of recording were discarded. Moreover, only units with clear refractory periods and well-defined cluster were included in the analyses. Recording sessions were divided into brain states of theta and slow oscillation periods. The epochs of stable slow oscillations (SO) periods were visually selected respectively from the ratios of the whitened power in the slow oscillations band (1-2 Hz) and the power of the

289 neighboring band (20-30 Hz) of mPFC or NR LFP and assisted by visual inspection of the raw
290 traces **(Quilichini et al., 2010)**.
291 Neurons were assigned as "NR neurons" by determining the approximate location of their
292 somata relative to the recording sites, the known distances between the recording sites, the
293 histological reconstruction of the recording electrode tracks and subsequent estimation of the
294 recording sites. All the neurons recorded from sites located near the close contour of the NR
295 were discarded. Neurons located at a minimal distance of 200µm of NR border and located
296 within contours of the ventro-median, submedian or antero-median thalamic nuclei were
297 classified as "other thalamic neurons" and used in the analysis **(Ferraris et al., 2018)**.

298 ## Data post-processing

299 From the spike times, the instantaneous firing rates of each cell was calculated by counting the
300 number of spikes inside a window of 50 ms, in overlapping intervals of 10 ms. The population
301 firing rate was estimated averaging the single cell firing rates at each 10ms interval. Both the
302 population rate and the single cell firing rate were smoothed with a Gaussian kernel of 5ms
303 width. Peaks of population activity (AP) were identified as the points where the population rate
304 amplitude was larger than the average rate plus 1 standard deviation. A separation between two
305 consecutive peaks of at least 600 ms was imposed on the peak detection algorithm to avoid
306 multiple peaks of activity within one up-state. For visualization purposes, all firing rate's heat
307 maps were normalized with the peak firing rate for each cell to guarantee a variation between
308 [0:1].

309 ## Phase analysis and sequence identification

310 LFP signals (from mPFC or NR) during slow oscillation phase were band-pass filtered between
311 0.5 Hz and 2 Hz with a second order Butterworth filter to extract only the UP/DOWN transitions.

The time evolution of the phase during the UP/DOWN cycle was extracted performing the Hilbert transform of the filtered LFP. We used Rayleigh circular statistics **(Ferraris et al., 2018, Berens, 2009)** to compute the mean phase at which each neuron fires ("preferred phase") and to build their firing-phase histograms (Figure 1Ba). For visualization purposes, the resulting histograms depicted in the heat maps were normalized with the peak value of the distribution. For each cell, we then calculated a resultant vector characterized by an angle describing the average preferred phase and a magnitude with values between [0 1], quantifying the coherence of the phases. The template order was obtained by organizing the average preferred phase in increasing order (0 to 2π).

Sequence reliability, sequence velocity and participation index

We extracted the UP state duration as described in **(Ferraris et al., 2018)**. At each UP state, the local activation order was calculated by measuring the time lag between the first activation of each neuron relative to the AP in a +/- 200ms window. Ordering the latencies in increasing order resulted in the local activation order. The reliability of a given sequence within a population peak was quantified as the Spearman rank correlation of the template order and the local activation order in that particular UP state. Sequences were considered reliable above 99% significance level. For each reliable sequence, the velocity of sequential activation was computed as the slope of a robust fit between the local activation order and the activation latency. To assess whether a neuron participated in a given sequence, the outliers in the robust fit were identified as those whose residual value were larger than twice the standard deviation of the residuals in the robust fit. The participation index is then calculated as the mean fraction of neurons that participated in the sequences of a recording session. A second linear fit between the local activation latency and the site of the linear probe closest to the neuron gives a measure of the

335 directionality of the sequence activation. A slope of the fit different than 0 implies an activation
336 towards a given direction. Since this slope has units of time/electrode site, we multiplied the
337 resulting value by 32 (the number of sites in the electrode) to account for the time required for a
338 sequence to travel along the electrode.

339 ## Activity peak triggered histogram (APTH)

340 Storing the values of activation time lag relative to the AP at each UP state allows us to compute
341 the so-called activity peak triggered histogram for each cell. With the APTH it is possible to
342 assess the statistics of the firing latencies in the neighborhood of the UP state (+/- 200 ms).
343 Once the APTH is obtained, one can calculate the variability of the activation lags as a measure
344 of the firing extent around the peak reported in Figure 3C. Variability of the APTH can be
345 calculated in analogy to the variance of a probability distribution function where τ is the mean
346 value of the APTH (See Figure 3C insert).

347 ## SPW-Rs detection and analysis

348 The procedure of SPW-Rs detection in the HPC stratum pyramidale LFP was based on those
349 described previously **(Ferraris et al., 2018, Isomura et al., 2006)**. Briefly, the LFP was digitally
350 bandpass filtered [80 250] Hz, and the power (root-mean-square) of the filtered signal was
351 calculated. The mean and SD of the power signal were calculated to determine the detection
352 threshold. Oscillatory epochs with a power of 5 or more SD above the mean were detected. The
353 beginning and the end of oscillatory epochs were marked at points where the power fell 0.5 SD.
354 Once the SPW-Rs were detected, the SPW-R half time was calculated as the average between
355 the start and the end of it. Then, the APTH for each cell was computed, taking each SPW-R half
356 time as the activity peak. To test whether a cell robustly participates in the SPW-Rs, we
357 compared the APTH against a uniform distribution with identical mean and standard deviation.

Cells whose APTH were different from the flat distribution above a 95% level were considered as robustly participating in the SPW-Rs. Cell participation ratio was obtained dividing the number of robustly participating neurons by the total number of recorded neurons for that session. Organizing the average time lag for robustly participating neurons in increasing order defined the template order for the ripple. For each SPW-R, the reliability of activation respect to the template was calculated via the Spearman rank correlation between the activation order of that SPW-R and the template order. To calculate this correlation, only the neurons that belong to the template order were considered. A correlation above 95% confidence interval was considered reliable.

Statistics

All results reported are based on a significance threshold $\alpha=0.05$, otherwise stated, and all groups included enough samples to enable rejection of the null hypothesis at that level. We used two sample Kolmogorov-Smirnov test to assess differences between distributions, and t-Student's test to evaluate differences in the mean of distributions. Correlation tests involving ranked variables (neuron indices and electrode sites) were performed via a Spearman rank correlation. We tested significant differences between percentages with a two proportion Z-test.

REFERENCES

Ali, M., Cholvin, T., Muller, M. A., Cosquer, B., Kelche, C., Cassel, J.-C. & Pereira De Vasconcelos, A. 2017. Environmental enrichment enhances systems-level consolidation of a spatial memory after lesions of the ventral midline thalamus. *Neurobiology of learning and memory,* **141,** 108-123. DOI: 10.1016/j.nlm.2017.03.021

379 Battaglia, F. P., Benchenane, K., Sirota, A., Pennartz, C. M. & Wiener, S. I. 2011. The
380 hippocampus: hub of brain network communication for memory. *Trends Cogn Sci,* **15,** 310-318.
381 DOI: 10.1016/j.tics.2011.05.008

382 Battaglia, F. P., Sutherland, G. R. & Mcnaughton, B. L. 2004. Hippocampal sharp wave bursts
383 coincide with neocortical "up-state" transitions. *Learning & memory,* **11,** 697-704. DOI:
384 10.1101/lm.73504

385 Berens, P. 2009. CircStat: A MATLAB Toolbox for Circular Statistics. *Journal of Statistical*
386 *Software,* **31,** 1-21. DOI: 10.18637/jss.v031.i10

387 Bermudez Contreras, E. J., Schjetnan, A. G. P., Muhammad, A., Bartho, P., Mcnaughton, B. L.,
388 Kolb, B., Gruber, A. J. & Luczak, A. 2013. Formation and reverberation of sequential neural
389 activity patterns evoked by sensory stimulation are enhanced during cortical desynchronization.
390 *Neuron,* **79,** 555-66. DOI: 10.1016/j.neuron.2013.06.013

391 Bokor, H., Csáki, A., Kocsis, K. & Kiss, J. 2002. Cellular architecture of the nucleus reuniens
392 thalami and its putative aspartatergic/glutamatergic projection to the hippocampus and medial
393 septum in the rat. *The European journal of neuroscience,* **16,** 1227-39. DOI: 10.1046/j.1460-
394 9568.2002.02189.x

395 Buzsáki, G. 2015. Hippocampal sharp wave-ripple: A cognitive biomarker for episodic memory
396 and planning. *Hippocampus,* **25,** 1073-188. DOI: 10.1002/hipo.22488

397 Cassel, J. C., Pereira De Vasconcelos, A., Loureiro, M., Cholvin, T., Dalrymple-Alford, J. C. &
398 Vertes, R. P. 2013. The reuniens and rhomboid nuclei: neuroanatomy, electrophysiological
399 characteristics and behavioral implications. *Progress in neurobiology,* **111,** 34-52. DOI:
400 10.1016/j.pneurobio.2013.08.006

401 Cholvin, T., Hok, V., Giorgi, L., Chaillan, F. A. & Poucet, B. 2018. Ventral Midline Thalamus Is
402 Necessary for Hippocampal Place Field Stability and Cell Firing Modulation. *J Neurosci,* **38,** 158-
403 172. DOI: 10.1523/JNEUROSCI.2039-17.2017

Clement, E. A., Richard, A., Thwaites, M., Ailon, J., Peters, S. & Dickson, C. T. 2008. Cyclic and sleep-like spontaneous alternations of brain state under urethane anaesthesia. *PloS one,* **3,** e2004-e2004. DOI: 10.1371/journal.pone.0002004

Csicsvari, J., Hirase, H., Czurko, A., Mamiya, A. & Buzsáki, G. 1999. Oscillatory coupling of hippocampal pyramidal cells and interneurons in the behaving Rat. *Journal of Neuroscience,* **19,** 274-287. DOI: 10.1523/JNEUROSCI.19-01-00274.1999

Davidson, T. J., Kloosterman, F. & Wilson, M. A. 2009. Hippocampal replay of extended experience. *Neuron,* **63,** 497-507. DOI: 10.1016/j.neuron.2009.07.027

Di Prisco, G. V. & Vertes, R. P. 2006. Excitatory actions of the ventral midline thalamus (rhomboid/reuniens) on the medial prefrontal cortex in the rat. *Synapse,* **60,** 45-55. DOI: 10.1002/syn.20271

Dolleman-Van Der Weel, M. J., Lopes Da Silva, F. H. & Witter, M. P. 1997. Nucleus reuniens thalami modulates activity in hippocampal field CA1 through excitatory and inhibitory mechanisms. *Journal of neuroscience,* **17,** 5640-50. DOI: 10.1523/JNEUROSCI.17-14-05640.1997

Dolleman-Van Der Weel, M. J. & Witter, M. P. 1996. Projections from the nucleus reuniens thalami to the entorhinal cortex, hippocampal field CA1, and the subiculum in the rat arise from different populations of neurons. *The Journal of comparative neurology,* **364,** 637-50. DOI: 10.1002/(SICI)1096-9861(19960122)364:4<637::AID-CNE3>3.0.CO;2-4

Dolleman-Van Der Weel, M. J. & Witter, M. P. 2000. Nucleus reuniens thalami innervates gamma aminobutyric acid positive cells in hippocampal field CA1 of the rat. *Neuroscience letters,* **278,** 145-8. DOI: 10.1016/S0304-3940(99)00935-0

Dragoi, G. & Buzsáki, G. 2006. Temporal encoding of place sequences by hippocampal cell assemblies. *Neuron,* **50,** 145-157. DOI: 10.1016/j.neuron.2006.02.023 [doi]

Dragoi, G. & Tonegawa, S. 2012. Preplay of future place cell sequences by hippocampal cellular assemblies. *Nature,* **469,** 397-401. DOI: 10.1038/nature09633

Eichenbaum, H. 2017. Prefrontal-hippocampal interactions in episodic memory. *Nature Rev. Neurosci.,* **18,** 547-558. DOI: 10.1038/nrn.2017.74

Euston, D. R., Tatsuno, M. & Mcnaughton, B. L. 2007. Fast-forward playback of recent memory sequences in prefrontal cortex during sleep. *Science,* **318,** 1147-50. DOI: 10.1126/science.1148979

Ferezou, I., Bolea, S. & Petersen, C. C. 2006. Visualizing the cortical representation of whisker touch: voltage-sensitive dye imaging in freely moving mice. *Neuron,* **50,** 617-29. DOI: 10.1016/j.neuron.2006.03.043

Ferraris, M., Ghestem, A., Vicente, A. F., Nallet-Khosrofian, L., Bernard, C. & Quilichini, P. P. 2018. The Nucleus Reuniens Controls Long-Range Hippocampo-Prefrontal Gamma Synchronization during Slow Oscillations. *J Neurosci,* **38,** 3026-3038. DOI: 10.1523/JNEUROSCI.3058-17.2018

Foster, D. J. & Wilson, M. A. 2006. Reverse replay of behavioural sequences in hippocampal place cells during the awake state. *Nature,* **440,** 680-683. DOI: 10.1038/nature04587 [doi]

Frankland, P. W. & Bontempi, B. 2005. The organization of recent and remote memories. *Nature Reviews Neuroscience,* **6,** 119-130. DOI: 10.1101/lm.97905

Harris, K. D., Csicsvari, J., Hirase, H., Dragoi, G. & Buzsáki, G. 2003. Organization of cell assemblies in the hippocampus. *Nature,* **424,** 552-556. DOI: 10.1038/nature01834

Hazan, L., Zugaro, M. & Buzsáki, G. 2006. Klusters, NeuroScope, NDManager: a free software suite for neurophysiological data processing and visualization. *J Neurosci Methods,* **155,** 207-216. DOI: 10.1016/j.jneumeth.2006.01.017

Herkenham, M. 1978. The connections of the nucleus reuniens thalami: evidence for a direct thalamo-hippocampal pathway in the rat. *The Journal of comparative neurology,* **177,** 589-610. DOI: 10.1002/cne.901770405

Hutt, A. 2011. *Sleep and Anesthesia; Neural correlates in Theory and experiment*, Springer. 10.1007/978-1-4614-0173-5: 10.1007/978-1-4614-0173-5

456 Isomura, Y., Sirota, A., Ozen, S., Montgomery, S., Mizuseki, K., Henze, D. A. & Buzsáki, G. 2006.
457 Integration and segregation of activity in entorhinal-hippocampal subregions by neocortical slow
458 oscillations. *Neuron,* **52,** 871-882. DOI: 10.1016/j.neuron.2006.10.023

459 Ito, H. T., Zhang, S.-J., Witter, M. P., Moser, E. I. & Moser, M.-B. 2015. A prefrontal–thalamo–
460 hippocampal circuit for goal-directed spatial navigation. *Nature,* **522,** 50-55. DOI:
461 10.1038/nature14396

462 Jankowski, M. M., Islam, M. N., Wright, N. F., Vann, S. D., Erichsen, J. T., Aggleton, J. P. &
463 O'mara, S. M. 2014. Nucleus reuniens of the thalamus contains head direction cells. *eLife,* **3,**
464 e03075-e03075. DOI: 10.7554/eLife.03075

465 Jankowski, M. M., Passecker, J., Islam, M. N., Vann, S., Erichsen, J. T., Aggleton, J. P. & O'mara,
466 S. M. 2015. Evidence for spatially-responsive neurons in the rostral thalamus. *Frontiers in*
467 *Behav. Neurosci.,* **9,** 256-256. DOI: 10.3389/fnbeh.2015.00256

468 Ji, D. & Wilson, M. A. 2007. Coordinated memory replay in the visual cortex and hippocampus
469 during sleep. *Nature Neuroscience,* **10,** 100-107. DOI: 10.1038/nn1825

470 Jones, E. G. 1985. *The Thalamus,* Plenum Press, New York 1985, Springer. 10.1007/978-1-
471 4615-1749-8: 10.1007/978-1-4615-1749-8

472 Kenet, T., Bibitchkov, D., Tsodyks, M., Grinvald, A. & Arieli, A. 2003. Spontaneously emerging
473 cortical representations of visual attributes. *Nature,* **425,** 954-6. DOI: 10.1038/nature02078

474 Khodagholy, D., Gelinas, J. N. & Buzsaki, G. 2017. Learning-enhanced coupling between ripple
475 oscillations in association cortices and hippocampus. *Science,* **358,** 369-372. DOI:
476 10.1126/science.aan6203

477 Kitamura, T., Ogawa, S. K., Roy, D. S., Okuyama, T., Morrissey, M. D., Smith, L. M., Redondo, R.
478 L. & Tonegawa, S. 2017. Engrams and circuits crucial for systems consolidation of a memory.
479 *Science,* **356,** 73-78. DOI: 10.1126/science.aam6808

480 Lansink, C. S., Goltstein, P. M., Lankelma, J. V., Mcnaughton, B. L. & Pennartz, C. M. 2009.
481 Hippocampus leads ventral striatum in replay of place-reward information. *PLoS Biol,* **7,**
482 e1000173-e1000173. DOI: 10.1371/journal.pbio.1000173

Latchoumane, C.-F. V., Ngo, H.-V. V., Born, J. & Shin, H.-S. 2017. Thalamic Spindles Promote Memory Formation during Sleep through Triple Phase-Locking of Cortical, Thalamic, and Hippocampal Rhythms. *Neuron,* **95,** 424-435. DOI: 10.1016/j.neuron.2017.06.025

Lee, A. K. & Wilson, M. A. 2002. Memory of sequential experience in the hippocampus during slow wave sleep. *Neuron,* **36,** 1183-1194. DOI: 10.1016/S0896-6273(02)01096-6

Liu, K., Sibille, J. & Dragoi, G. 2018. Preconfigured patterns are the primary driver of offline multi-neuronal sequence replay. *Hippocampus*. DOI: 10.1002/hipo.23034

Loureiro, M., Cholvin, T., Lopez, J., Merienne, N., Latreche, A., Cosquer, B., Geiger, K., Kelche, C., Cassel, J.-C. & Pereira De Vasconcelos, A. 2012. The ventral midline thalamus (reuniens and rhomboid nuclei) contributes to the persistence of spatial memory in rats. *Journal of Neuroscience,* **32,** 9947-59. DOI: 10.1523/JNEUROSCI.0410-12.2012

Luczak, A., Bartho, P., Marguet, S. L., Buzsáki, G. & Harris, K. D. 2007. Sequential structure of neocortical spontaneous activity in vivo. *PNAS,* **104,** 347-352. DOI: 10.1073/pnas.0605643104

Luczak, A. & Maclean, J. N. 2012. Default activity patterns at the neocortical microcircuit level. *Frontiers in integrative neuroscience,* **6,** 30-30. DOI: 10.3389/fnint.2012.00030

Luczak, A., Mcnaughton, B. L. & Harris, K. D. 2015. Packet-based communication in the cortex. *Nature Reviews Neuroscience,* **16,** 745-755. DOI: 10.1038/nrn4026

Maass, W. 2016. Searching for principles of brain computation. *Current Opinion in Behavioral Sciences,* **11,** 81-92. DOI: 10.1016/j.cobeha.2016.06.003

Maclean, J. N., Watson, B. O., Aaron, G. B. & Yuste, R. 2005. Internal dynamics determine the cortical response to thalamic stimulation. *Neuron,* **48,** 811-23. DOI: 10.1016/j.neuron.2005.09.035

Maingret, N., Girardeau, G., Todorova, R., Goutierre, M. & Zugaro, M. 2016. Hippocampo-cortical coupling mediates memory consolidation during sleep. *Nature neuroscience,* **19,** 959-64. DOI: 10.1038/nn.4304

508 Malvache, A., Reichinnek, S., Villette, V., Haimerl, C. & Cossart, R. 2016. Awake hippocampal
509 reactivations project onto orthogonal neuronal assemblies. *Science,* **353,** 1280-3. DOI:
510 10.1126/science.aaf3319

511 Marre, O., Yger, P., Davison, A. P. & Frégnac, Y. 2009. Reliable Recall of Spontaneous Activity
512 Patterns in Cortical Networks. *Journal of Neuroscience,* **29,** 14596-14606. DOI:
513 10.1523/JNEUROSCI.0753-09.2009

514 Mckenna, J. T. & Vertes, R. P. 2004. Afferent projections to nucleus reuniens of the thalamus.
515 *The Journal of comparative neurology,* **480,** 115-42. DOI: 10.1002/cne.20342

516 Nádasdy, Z. 2000. Spike sequences and their consequences. *Journal of physiology, Paris,* **94,**
517 505-24. DOI: 10.1016/S0928-4257(00)01103-7

518 Nadasdy, Z., Hirase, H., Czurko, A., Csicsvari, J. & Buzsáki, G. 1999. Replay and time
519 compression of recurring spike sequences in the hippocampus. *Journal of Neuroscience,* **19,**
520 9497-9507. DOI: 10.1523/JNEUROSCI.19-21-09497.1999

521 Pastalkova, E., Itskov, V., Amarasingham, A. & Buzsáki, G. 2008. Internally generated cell
522 assembly sequences in the rat hippocampus. *Science,* **321,** 1322-1327. DOI:
523 10.1126/science.1159775

524 Pereira De Vasconcelos, A. & Cassel, J.-C. 2015. The nonspecific thalamus: A place in a
525 wedding bed for making memories last? *Neurosci. & biobehav. rev.,* **54,** 175-96. DOI:
526 10.1016/j.neubiorev.2014.10.021

527 Peyrache, A., Khamassi, M., Benchenane, K., Wiener, S. I. & Battaglia, F. P. 2009. Replay of rule-
528 learning related neural patterns in the prefrontal cortex during sleep. *Nature neuroscience,* **12,**
529 919-26. DOI: 10.1038/nn.2337

530 Pfeiffer, B. E. 2017. The Content of Hippocampal "Replay". *Hippocampus*, 1-13. DOI:
531 10.1002/hipo.22824

532 Preston, A. R. & Eichenbaum, H. 2013. Interplay of hippocampus and prefrontal cortex in
533 memory. *Current biology : CB,* **23,** R764-73. DOI: 10.1016/j.cub.2013.05.041

534 Quilichini, P., Sirota, A. & Buzsáki, G. 2010. Intrinsic circuit organization and theta-gamma
535 oscillation dynamics in the entorhinal cortex of the rat. *J Neurosci,* **30,** 11128-11142. DOI:
536 10.1523/JNEUROSCI.1327-10.2010

537 Sanchez-Vives, M. V. & Mattia, M. 2014. Slow wave activity as the default mode of the cerebral
538 cortex. *Archives Italiennes de Biologie,* **152,** 147-155. DOI: 10.12871/000298292014239

539 Siapas, A. G. & Wilson, M. A. 1998. Coordinated interactions between hippocampal ripples and
540 cortical spindles during slow-wave sleep. *Neuron,* **21,** 1123-8. DOI: S0896-6273(00)80629-7

541 Sirota, A. & Buzsáki, G. 2005. Interaction between neocortical and hippocampal networks via
542 slow oscillations. *Thalamus & related systems,* **3,** 245-259. DOI: 10.1017/S1472928807000258

543 Sirota, A., Csicsvari, J., Buhl, D. & Buzsáki, G. 2003. Communication between neocortex and
544 hippocampus during sleep in rodents. *PNAS,* **100,** 2065-9. DOI: 10.1073/pnas.0437938100

545 Skaggs, W. E. & Mcnaughton, B. L. 1996. Replay of neuronal firing sequences in rat
546 hippocampus during sleep following spatial experience. *Science,* **271,** 1870-1873. DOI:
547 10.1126/science.271.5257.1870

548 Staresina, B. P., Ole Bergmann, T., Bonnefond, M., Van Der Meij, R., Jensen, O., Deuker, L.,
549 Elger, C. E., Axmacher, N. & Fell, J. 2015. Hierarchical nesting of slow oscillations, spindles and
550 ripples in the human hippocampus during sleep. *Nature Neuroscience,* **18,** 1679-1686. DOI:
551 10.1038/nn.4119

552 Tonegawa, S., Morrissey, M. D. & Kitamura, T. 2018. The role of engram cells in the systems
553 consolidation of memory. *Nat Rev Neurosci,* **19,** 485-498. DOI: 10.1038/s41583-018-0031-2

554 Tung, A. & Mendelson, W. B. 2004. Anesthesia and sleep. *Sleep Med Rev,* **8,** 213-25. DOI:
555 10.1016/j.smrv.2004.01.003

556 Van Der Werf, Y. D., Witter, M. P. & Groenewegen, H. J. 2002. The intralaminar and midline
557 nuclei of the thalamus. Anatomical and functional evidence for participation in processes of
558 arousal and awareness. *Brain Res Brain Res Rev,* **39,** 107-140. DOI: S0165017302001819

559 Varela, C., Kumar, S., Yang, J. Y. & Wilson, M. A. 2014. Anatomical substrates for direct
560 interactions between hippocampus, medial prefrontal cortex, and the thalamic nucleus reuniens.
561 *Brain Struct Funct,* **219,** 911-29. DOI: 10.1007/s00429-013-0543-5

562 Vertes, R. P. 2006. Interactions among the medial prefrontal cortex, hippocampus and midline
563 thalamus in emotional and cognitive processing in the rat. *Neuroscience,* **142,** 1-20. DOI:
564 10.1016/j.neuroscience.2006.06.027

565 Vertes, R. P., Hoover, W. B., Do Valle, A. C., Sherman, A. & Rodriguez, J. J. 2006. Efferent
566 projections of reuniens and rhomboid nuclei of the thalamus in the rat. *The Journal of*
567 *comparative neurology,* **499,** 768-96. DOI: 10.1002/cne.21135

568 Villette, V., Malvache, A., Tressard, T., Dupuy, N., Villette, V., Malvache, A., Tressard, T., Dupuy,
569 N. & Cossart, R. 2015. Internally Recurring Hippocampal Sequences as a Population Template
570 of Spatiotemporal Information Article Internally Recurring Hippocampal Sequences as a
571 Population Template of Spatiotemporal Information. *Neuron,* **88,** 357-366. DOI:
572 10.1016/j.neuron.2015.09.052

573 Walsh, D. A., Brown, J. T. & Randall, A. D. 2017. In vitro characterization of cell-level
574 neurophysiological diversity in the rostral nucleus reuniens of adult mice. *J Physiol,* **595,** 3549-
575 3572. DOI: 10.1113/JP273915

FIGURES & FIGURE LEGENDS

Figure 1. Sequential dynamics of cell assemblies.

A) Two template heat maps of normalized NR unit activities (top) with **(a)** mPFC or **(b)** HPC normalized unit activities showing the repetition of neuronal assemblies particularly in NR and mPFC. The upper trace depicts the [0.5-2] Hz filtered LFP in **(a)** mPFC and **(b)** NR, where the UP states correspond to troughs in the LFP signal.

B) (a) Phase distribution of the NR, mPFC, HPC and TH population firing (grouped data) as a reference to SO phase (depicted by the dashed curve). **(b)** Heat maps of normalized distribution of neurons preferred SO phase for NR, mPFC, HPC and TH. The activation order for each neuron is calculated as the average preferred phase. Heat maps are ordered according to the increasing value of average preferred phase (colored circles), defining the sequential activation template.

C) Percentage of reliable sequences detected in the NR, mPFC, HPC and TH.

D) Average Spearman correlation of reliable sequences only found in NR and mPFC.

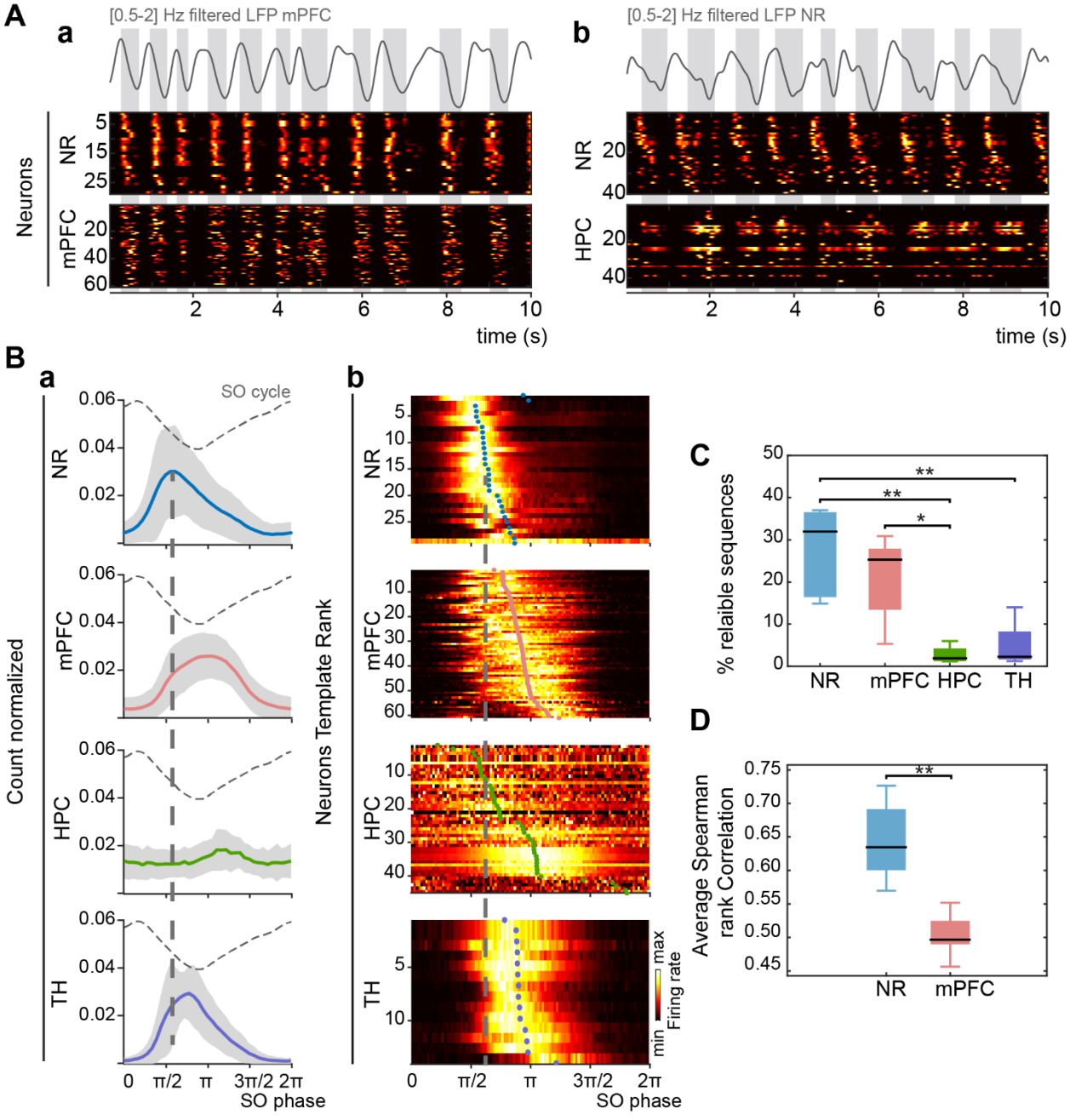

590

591 *Figure 1. Sequential dynamics of cell assemblies.*

Figure 2. Spatial organization of NR and mPFC cell assemblies.

A) Representation of the position of a linear silicon probe with 32 recording sites in **(a)** the NR and **(b)** mPFC. NR and mPFC contours (and layers) are delimited by the white dashed line over the green fluorescent Nissl staining (fmi: forceps minor of the corpus callosum; 3rd V: third ventricle; PrL: prelimbic area; IL: infralimbic area). The red-orange staining corresponds to the DiI that was deposited at the back of the silicon probe before insertion (D: dorsal; L: lateral).

B) Relationship between anatomical dorso-ventral location of NR (left panel) and mPFC (right panel) neurons (location defined by the site of the probe recording the maximum amplitude of the action potentials) and the template rank showing a linear correlation for NR neurons but not for mPFC ones in a template experiment.

C) Distribution of spatial propagation velocities across the probe for a template simultaneous recording of mPFC (red) and NR (blue) neurons.

D) Mean propagation time across experiments for NR and mPFC.

E) Percentage of spatially propagating cases found in NR and mPFC.

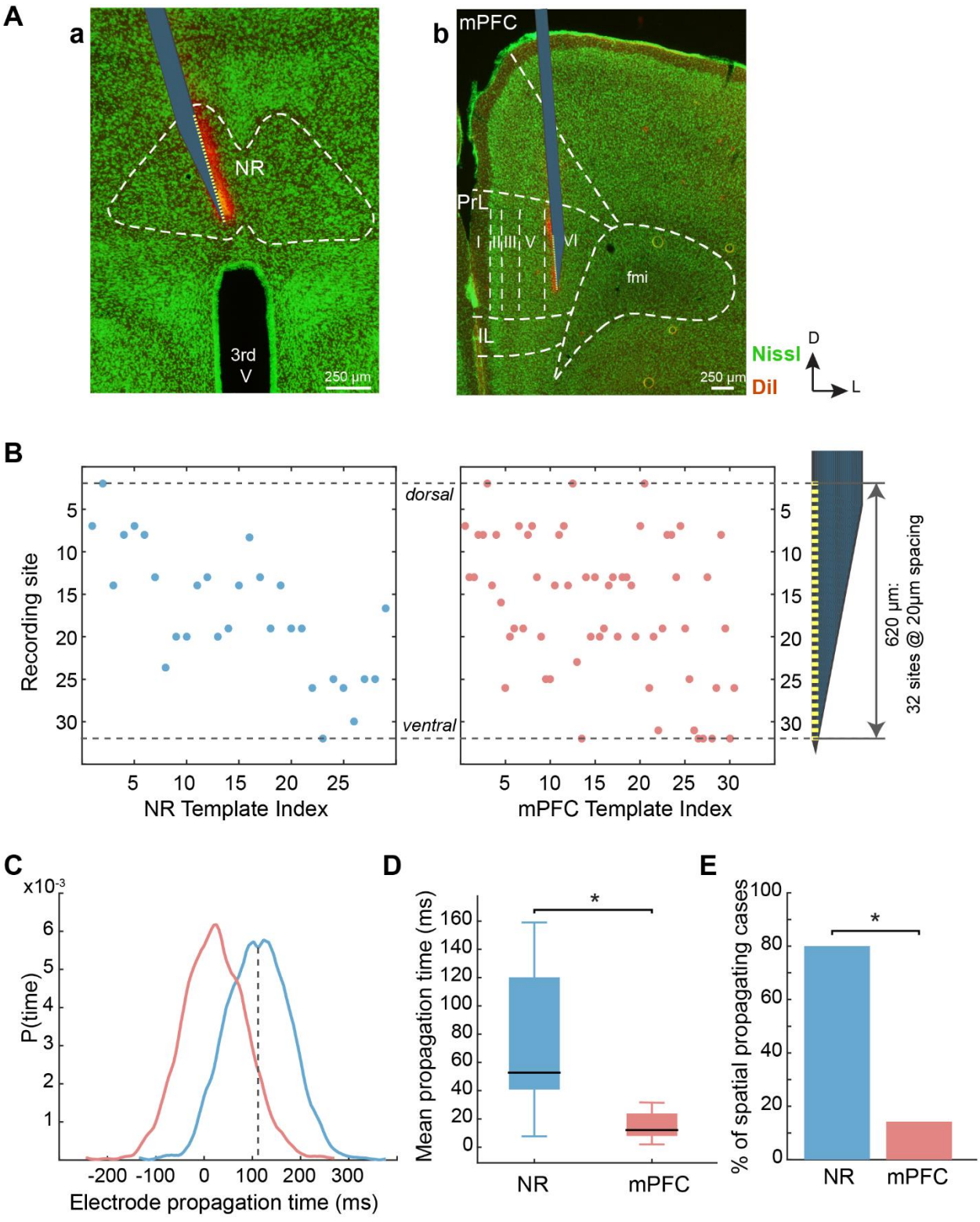

606

607 *Figure 2. Spatial organization of NR and mPFC cell assemblies.*

Figure 3. Inactivation of NR impairs reliable sequential activation of mPFC neurons at the beginning of the UP state.

A) Two template heat maps of normalized mPFC unit activities in control and during NR inactivation condition showing less stable cell assemblies. The upper traces depict the [0.5-2] Hz filtered LFP in mPFC, where the UP states correspond to troughs in the LFP signal.

B) Inter-spike interval distribution of mPFC neurons grouped data for control (red) and NR inactivation condition (purple).

C) Grouped data of the variability of the APTH for control (CTR) and NR inactivation conditions (MSCI). Insert: APTH: the activity peak triggered histogram quantifies the lag distribution with respect to the population activity peak for each neuron.

D) Distribution of the duration of the UP state in control (red) and NR inactivation (purple) condition, where a peak at short values indicates the emergence of shorter UP states.

E) Number of reliable sequences found in mPFC when NR is inactivated (MSCI) as compared to control (CTR) condition (grouped data, n=3 experiments).

F) Neurons participation to the reliable sequences (MSCI versus CTR, grouped data).

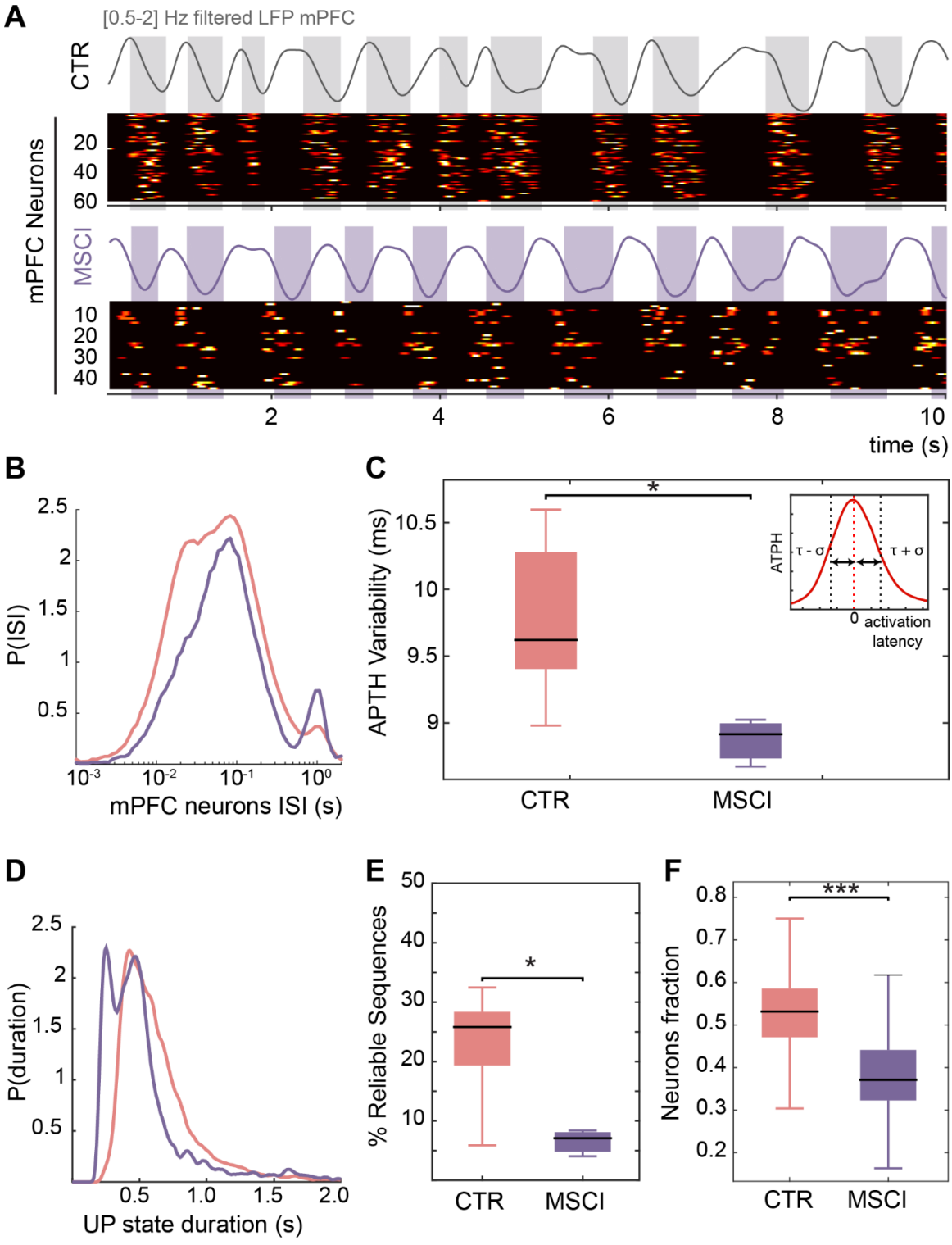

623

624 *Figure 3. Inactivation of NR impairs reliable sequential activation of mPFC neurons at*

625 *the beginning of the UP state.*

Figure 4: Inactivation of NR impairs reliable sequential activation of HPC neurons during SPW-Rs.

A) Two template heat maps of normalized HPC unit activities in control (CTR) and NR inactivation (MSCI) condition. The upper traces depict the [0.5-2] Hz filtered LFP in mPFC, where the UP states correspond to troughs in the LFP signal, and the black arrow mark the presence of a SPW-R event.

B) SPW-Rs occurrence is not changed when NR is inactivated (grouped data, n=3 experiments, n=913 SPW-R events in CTR, n=89 SPW-R events in MSCI).

C) SPW-R events normalized power and inner frequency in control versus NR inactivation conditions.

D) Proportion of reliable cell assemblies during SPW-Rs in control (CTR) and NR inactivation (MSCI) condition.

E) Fraction of reliably participating HPC neurons to sequences during SPW-R events in control and NR inactivation conditions.

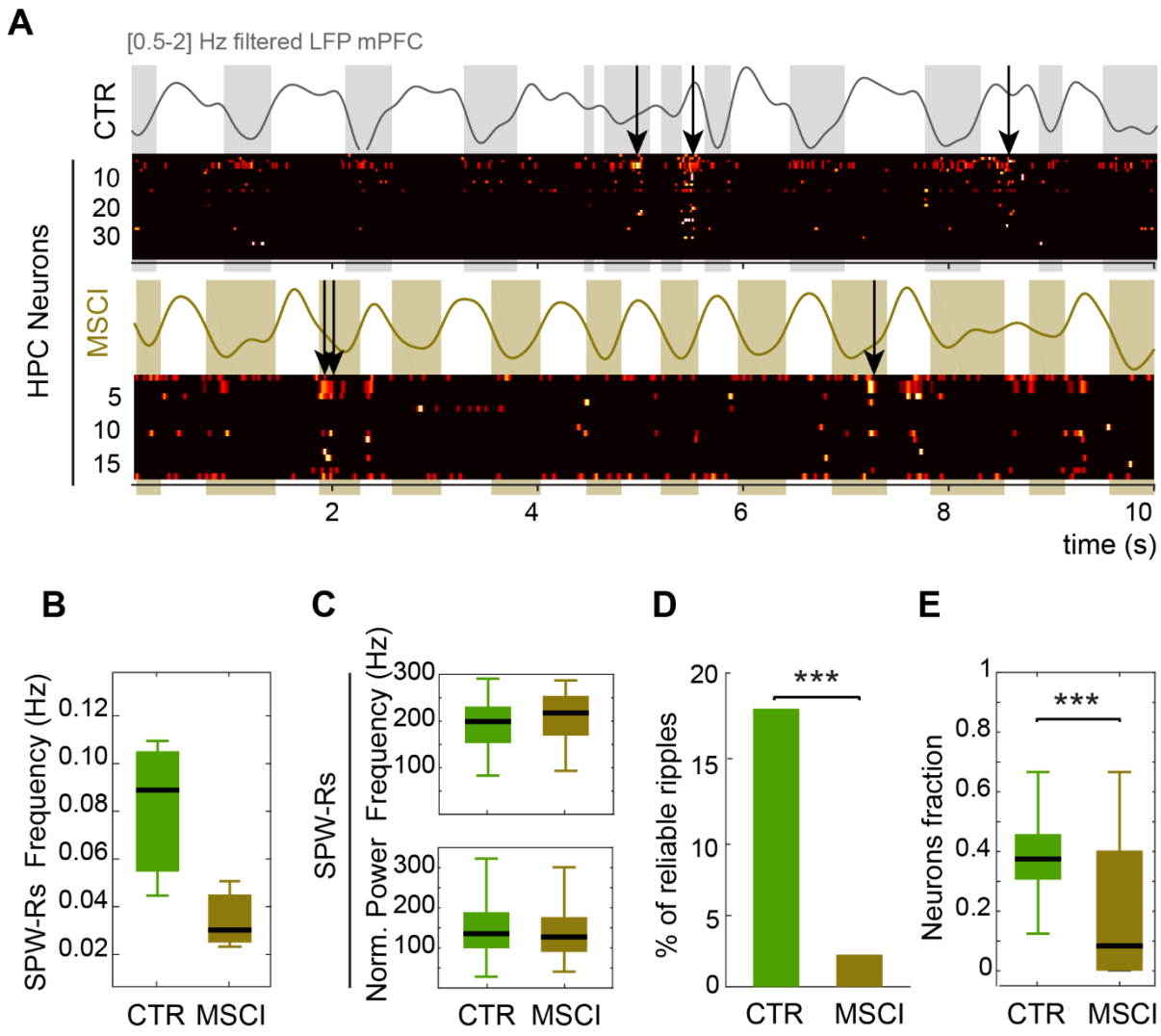

640

641 *Figure 4: Inactivation of NR impairs reliable sequential activation of HPC neurons during*

642 *SPW-Rs.*